Hindawi
Journal of Sensors
Volume 2018, Article ID 7497619, 14 pages
https://doi.org/10.1155/2018/7497619

Research Article

Enhanced Ammonia Adsorption on Directly Deposited Nanofibrous Carbon Films

Alexander G. Bannov,[1,2] **Ondřej Jašek**,[3] **Jan Prášek**,[4,5] **Jiří Buršík**,[6] **and Lenka Zajíčková**[1,3]

[1]*Central European Institute of Technology, Masaryk University, Kamenice 5, CZ-62500 Brno, Czech Republic*
[2]*Department of Chemistry and Chemical Technology, K. Marx 20, Novosibirsk State Technical University, 630073 Novosibirsk, Russia*
[3]*Department of Physical Electronics, Faculty of Science, Masaryk University, Kotlářská 2, CZ-61137 Brno, Czech Republic*
[4]*Central European Institute of Technology, Brno University of Technology, Technická 3058/10, CZ-61600 Brno, Czech Republic*
[5]*Centre of Sensors, Information and Communication Systems, Faculty of Electrical Engineering and Communication, Technická 3058/10, CZ-61600 Brno, Czech Republic*
[6]*Institute of Physics of Materials, Academy of Sciences of the Czech Republic, Žižkova 22, CZ-61662 Brno, Czech Republic*

Correspondence should be addressed to Alexander G. Bannov; bannov_a@mail.ru

Received 12 April 2018; Revised 9 July 2018; Accepted 29 July 2018; Published 17 September 2018

Academic Editor: Michele Penza

The ammonia adsorption on the nanostructured carbon thin film was significantly influenced by the choice of deposition temperature and deposition time of thin film synthesis. The thin films were prepared on Si/SiO_2 substrates by chemical vapour deposition in Ar/C_2H_2 gas mixture using iron catalytic nanoparticles. The analysis of the grown layer by the scanning and transmission electron microscopy showed the transition from long multiwalled nanotubes (MWCNTs) to bamboo-like hollow carbon nanofiber structure with the decrease of the deposition temperature from 700 to 600°C. Further, the material was analyzed by energy-dispersive X-ray spectroscopy and Raman spectroscopy confirmed the transition from graphitic sp^2 structure to highly defective structure at lower deposition temperature. The resistance of the prepared layer strongly depends on deposition temperature (T_d) and deposition time (t_d). High resistance layer, 38.6 kΩ, was formed at T_d 600°C and t_d 10 min, while at T_d 700°C and t_d 60 min, the resistance decreased to 860 ohms. Such behaviour is consistent with MWCNTs being responsible for the formation of the conductive network. Such system was studied using chemiresistor ammonia gas sensor configuration. The sensor resistance increased when exposed to ammonia in all the cases, but their response varied considerably. A decrease in deposition time, from 60 to 10 min, and the deposition temperature, from 700 to 600°C, led to the 10-fold increase in the sensor response. The measurements carried out at room temperature showed the higher sensor response than the measurements carried out at 200°C. This behaviour can be explained by the change in adsorption-desorption equilibrium at different temperatures. Analysis of dependence of the sensor response on the ammonia concentration proved that the underlying resistance change mechanism is chemisorption of ammonia molecules on the carbon network corresponding to the Langmuir isotherm.

1. Introduction

A safety and sustainable development require creation of new highly sensitive devices for the detection of toxic and flammable gases along with the control of environmental pollution. Such devices require new materials which extend the number of detectable gases and lower their detection limits. One of the most dangerous gases that have a negative influence on human health and environment is ammonia (NH_3). According to US OHSA (Occupational Safety and Health Administration) and CDC (Centers for Disease Control and Prevention) regulations, the long-term exposure limits are 25–35 ppm for

workers. The smell threshold of ammonia ranges from 5 to 15 ppm. The concentrations above 50 ppm induce irritation to the mouth, nose, wheezing, etc. The concentrations from 300 to 500 ppm are dangerous for life. In industry, ammonia can be detected at higher concentrations (from 1000 ppm to 40000 ppm, depending on rooms, facilities, etc.).

Therefore, study of ammonia adsorption on nanostructured surfaces and development of new materials for ammonia gas sensors attracted a lot of attention of scientific community. Single-wall carbon nanotubes (SWCNTs) and multiwall carbon nanotubes (MWCNTs) belong to one of the most promising candidates in the gas sensing field [1–9] because of their ability to change the electrical properties (e.g., resistivity) under gas adsorption. This fact is complemented by the enhanced adsorption of gases by carbon nanomaterials [8]. There are a wide range of gases on which the carbon nanotube- (CNT-) based sensors can be used, such as NH_3 [4, 10–16], NO_2 [17, 18], CH_4 [19, 20], H_2 [21], H_2S [22–25], CO_2 [26], ethanol [25], methanol [25], hydrocarbons [7], and other gases.

Commercially available sensors require a high temperature for their operation. For wider use of such devices, the room temperature operation of ammonia gas sensors is an important requirement and was recently studied by several authors. In [27], the authors created HCl-doped MWCNT/polyaniline composite sensors with good sensing response and high reproducibility. In [28], the authors created SWCNT- (40% metallic and 60% semiconducting) based ammonia sensors using inkjet-printed electrodes which possessed the maximal response of 27.3% for 500 ppm at room temperature. Cui et al. [29] developed the room temperature ammonia sensor based on Ag nanocrystal-functionalized MWCNTs that exhibited enhanced response of 9% and fast response at room temperature with the full recovery within several minutes in air. In [12], the authors created the room temperature sensor based on SWCNT for ammonia sensing with the extremely low detection limit (3 ppb). The enhancement of the response was realized by two techniques: drop casting and sonication.

In this paper, a promising potential of managing the NH_3 gas sensor performance by the control of nanofibrous carbon (NFC) chemical vapour deposition (CVD) synthesis conditions is investigated in detail. Up to now, the CNT-based NH_3 gas sensors were closely investigated from the performance point of view but the influence of the synthesis conditions of these materials on the sensing properties has not yet been studied. Previous studies were based on the creation of the sensors by the direct deposition of CNTs using only certain conditions [30–33] without detailed investigation of their synthesis role in the formation of sensor response. The influence of NFC deposition parameters (growth temperature and time) on the materials' properties and NH_3 sensing characteristics is determined. The interconnection between the sensor resistance and response has been found.

2. Materials and Methods

2.1. Nanofibrous Carbon Film Preparation. NFC layers were grown by atmospheric pressure chemical vapour deposition using an iron catalyst. Polished single-crystal Si (c-Si) pieces (8 mm × 8 mm) coated by a thermal SiO_2 film, 92 nm in thickness, were used as substrates. Nanoparticles (NPs) of iron catalyst were deposited by a microwave (MW) plasma torch from the iron pentacarbonyl, $Fe(CO)_5$, vapours mixed with argon. The experimental set-up is described by Synek et al. [34, 35] in detail. The c-Si/SiO_2 substrates were put in a special holder for 4 samples. The flow rate of argon through the central part of the nozzle was 700 sccm. The outer concentric part of the nozzle was used to deliver $Fe(CO)_5$ vapours (0.1 sccm) carried by Ar flow of 28 sccm. The MW torch was ignited with the power of 210 W. The deposition time of the nanoparticles was 15 s. Direct deposition of nanoparticles was used as preferred form of the catalyst because it enabled us to form a sparse network of fibrous carbon. In case of the thin film catalyst, dense structure of the nanofibrous carbon network with low resistance and negligible response was formed.

Table 1: Summary of conditions used for the growth of NFC by CVD.

Sample	Reduction and deposition temperature (T_d), °C	Reduction time, min	Deposition time (t_d), min
CNF600-10	600	10	10
CNF600-40	600	10	40
CNF600-60	600	10	60
CNF650-10	650	10	10
CNF650-40	650	10	40
CNF650-60	650	10	60
CNF700-10	700	10	10
CNF700-40	700	10	40
CNF700-60	700	10	60

NFC growth was carried out in a quartz tubular furnace. The processes started by heating the furnace from the room temperature to deposition temperature (T_d): 600°C, 650°C, and 700°C, under the argon flow of 1400 sccm. The heating speed was 25°C/min. Then, the catalytic nanoparticles were reduced in Ar/H_2 flow (1400 sccm of Ar and 500 sccm of H_2) for 10 min. After reduction, the hydrogen flow was switched off and NFC growth was carried out in Ar/C_2H_2 mixture with the flow rates of 1400 and 25 sccm, respectively. The growth lasted for 10 min, 40 min, and 60 min as summarized in Table 1.

The reactor was cooled down to the room temperature under argon flow. The samples were taken out and placed in a vacuum evaporator for the deposition of 6.65 mm × 2.33 mm gold contacting pads overlapping by 1 mm with the field of NFC (Figure 1). Thickness of the Au layer was 350 nm, and a 15 nm thick Ni/Cr layer was used to improve Au adhesion to the substrate. Such prepared substrates were used as sensors for measurement of resistance change under various gas atmospheres.

2.2. Investigation Methods of NFC Films. The as-prepared catalytic NPs and NFCs on c-Si/SiO_2 substrates were investigated by scanning electron microscopy (SEM) with MIRA II

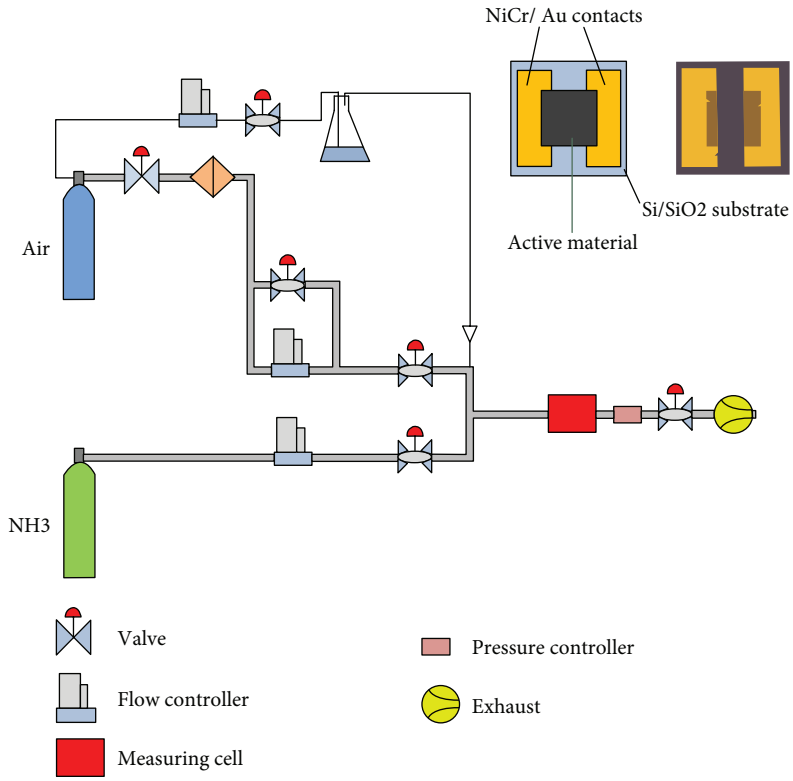

Figure 1: The sensor layout and experimental set-up for measurement of sensor response to ammonia.

(TESCAN, Brno, Czech Republic) equipped with the EDX detector (Oxford Instruments, UK). Raman spectra of NFCs were obtained using the Renishaw inVia (Renishaw, Gloucestershire, UK) spectrometer in the range 100–3200 cm^{-1} ($\lambda = 514$ nm). Raman spectra were treated using Lorentzian fitting. Structure and morphology of carbon nanomaterials and catalytic nanoparticles were additionally investigated using the CM12 STEM transmission electron microscope (Philips, Eindhoven, Netherlands).

Gas sensing characteristics of the sensors were determined by measuring the changes of sensor resistance during ammonia exposure in a custom-built system equipped with two gas channels and a measurement chamber (Figure 1). Synthetic air (80% N_2, 20% O_2, Linde, Brno, Czech Republic) was used as a gas carrier in one gas channel. Along with it, the second gas line was flowed by ammonia diluted in nitrogen (calibration gas 5000 ppm of NH_3 in N_2, Linde, Brno, Czech Republic). Total volume flow rate of gases was set constant at 500 sccm for all stabilizations and measurements, but the concentration of NH_3 in the mixture with synthetic air and N_2 was changed. The additional channel for oxygen was used in the setup, and oxygen was admixed when increasing ammonia concentration in order to keep the concentration of air and nitrogen mixture the same as in synthetic air.

Gas distribution system was made of stainless steel (connections, tubes). The volume of the chamber where the sensors were examined was 160 cm^3 (length: 10 cm, width: 8 cm, height: 2 cm).

The sensor was placed on a heater inside the measurement chamber, and the measurements were carried out at two temperatures: room temperature ($25 \pm 2^{\circ}C$) and 200°C ($\pm 2^{\circ}C$). The heating temperature was controlled by the DC power supply Agilent U3606A (Agilent, Santa Clara, California, USA) using temperature calibration curves. The resistance was measured by two electrodes that were placed to Au pads. Electrodes were plugged to a high voltage source meter Keithley 2410 (Keithley, Cleveland, OH, USA) using 1 V bias voltage. In the present work, no efforts were made to dope or treat NFCs for response enhancement. Solely, the correlations between the NFC deposition conditions, influencing the structure and composition of the deposit, and the gas sensor properties were investigated. Relative humidity (RH) in the chamber was controlled by the SHT25 sensor (Sensirion, Staefa, Switzerland). Also, the measurements of humidity influence on sensing properties were carried out. The level of RH during measuring the response in dry gases from cylinders was 2.5–3%. The measurements in different RH conditions were carried out by feeding the wet air to the chamber additionally with dry air and analyte.

Before each response measurement, the sensor was conditioned and recovered for 30 min at 200°C in the synthetic air flow of 1000 sccm. The baseline of the sensor resistance was stabilized at desired temperature in 500 sccm synthetic air flow for 60 min before the first measurement of each sample. After the baseline stabilization, the sensor response to NH_3 was measured using alternating cycles, 10 min in synthetic air and 10 min in the mixture of the NH_3 with synthetic air. This cycle was repeated for several tested concentrations, 100 ppm, 250 ppm, and 500 ppm of NH_3.

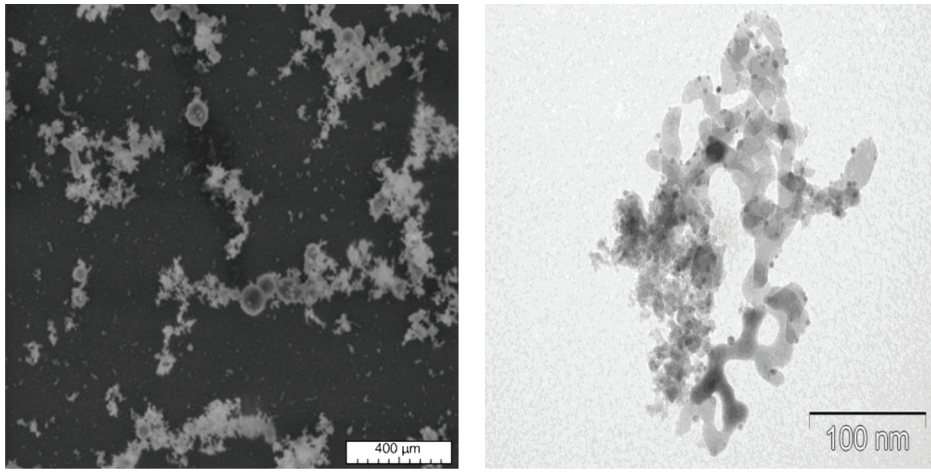

(a) (b)

Figure 2: SEM (a) and TEM (b) micrographs of catalytic nanoparticles synthesized by the MW torch.

The baseline resistance, R_0, was linearly extrapolated along the measurement time, and the sensor response was determined by subtracting the baseline resistance signal from the sample resistance under ammonia exposure, R. The measurement of baseline and extrapolation has been done for each measurement of all samples. The sensor response was defined as follows:

$$\frac{\Delta R}{R_0} = \left(\frac{(R - R_0)}{R_0}\right) \cdot 100\%. \quad (1)$$

The instrumental detection limit of the sensor response was 10 ppm, the value was limited by the flow controller characteristics (low accuracy of flow rate control at the value up to 1 sccm) for the sensor measurement. To estimate the sensor selectivity, they were also tested for detection of H_2 and iC_4H_{10}. These gases were also fed diluted in N_2 (5000 ppm of NH_3). The resolution of scanning of sensor resistance was 0.5 s (one experimental point per 0.5 s).

3. Results and Discussion

3.1. Characterization of Catalytic Nanoparticles and Carbon Nanostructures. The typical SEM and TEM micrographs of catalytic nanoparticles are shown in Figure 2. The catalyst formed aggregates consisting of nanoparticles with the size of 5–25 nm. It was difficult to determine the phase composition of the catalyst by X-ray diffraction or Raman spectroscopy because of the low amount of nanoparticles on the substrate. Therefore, the phase composition was studied by electron diffraction in TEM. The analyses revealed that the catalyst consisted of iron oxides, predominantly maghemite (γ-Fe_2O_3). Maghemite (γ-Fe_2O_3) phase was detected (Figure S1 Supplementary Materials) by selected area electron diffraction (SAED) by TEM. It is in agreement with the data obtained by Synek et al. [34].

The SEM and TEM micrographs of the NFCs grown for 10 min at 600°C (Figure 3) show both the typical hollow carbon structures observed also in other samples, long MWCNTs (2–5 μm) with walls consisting of graphene layers parallel to the tube axis, and strongly curved short bamboo-like hollow structures. Besides, the samples contained also carbon-encapsulated Fe and Fe_3C nanoparticles.

The diameter of MWCNTs, 10–30 nm, suggests that the growth was initiated from small, 5–25 nm, catalytic NPs. The bamboo-like structures, 50–120 nm in diameter, are expected to grow from larger NPs (>45 nm in diameter). The difference in their growth mechanism, as compared to MWCNTs, induces a strong curvature with chain-like morphology that has some similarities to CNFs [36]. Initially, a higher amount of small NPs, a lower activity of large NPs, and limited growth time were the reasons for much higher amount of MWCNTs than bamboo-like CNFs on the substrates (Figure 3(a)) [37].

SEM micrographs of the NFC samples prepared at different temperatures and times are presented in Figure S2 (Supplementary Materials). At 600°C, the increased deposition times, 40 and 60 min, led to the growth of longer nanotubes and a formation of more dense nanotube aggregates compared to 10 min. According to EDX analysis of the CNF600-10 sample, the C/Fe weight ratio was 26.5 and it increased to 85 and 107 with increasing deposition time for CNF600-40 and CNF600-60 samples, respectively. At higher temperatures (650, 700°C), the yield of CNT increased and a denser MWCNT network was formed.

Raman spectroscopy of all the NFC samples was carried out for assessing the overall structure of the deposits. Raman spectra for the CNF600-10, CNF650-10, and CNF700-10 samples are shown in Figure 4(a). The spectra were dominated by two peaks corresponding to disordered D and graphitic G bands [38]. The positions of the D and G peaks ranged from 1349 to 1352 cm^{-1} and from 1581 to 1594 cm^{-1}, respectively (Table 2).

The second-order peaks were presented above 2500 cm^{-1}. The peaks of silicon at 520 cm^{-1} and 960 cm^{-1} were observed in case of sparsely coated substrates (low growth of temperature and time). The ratio of D and G peak intensities, $I(D)/I(G)$, provided information about material's disorder

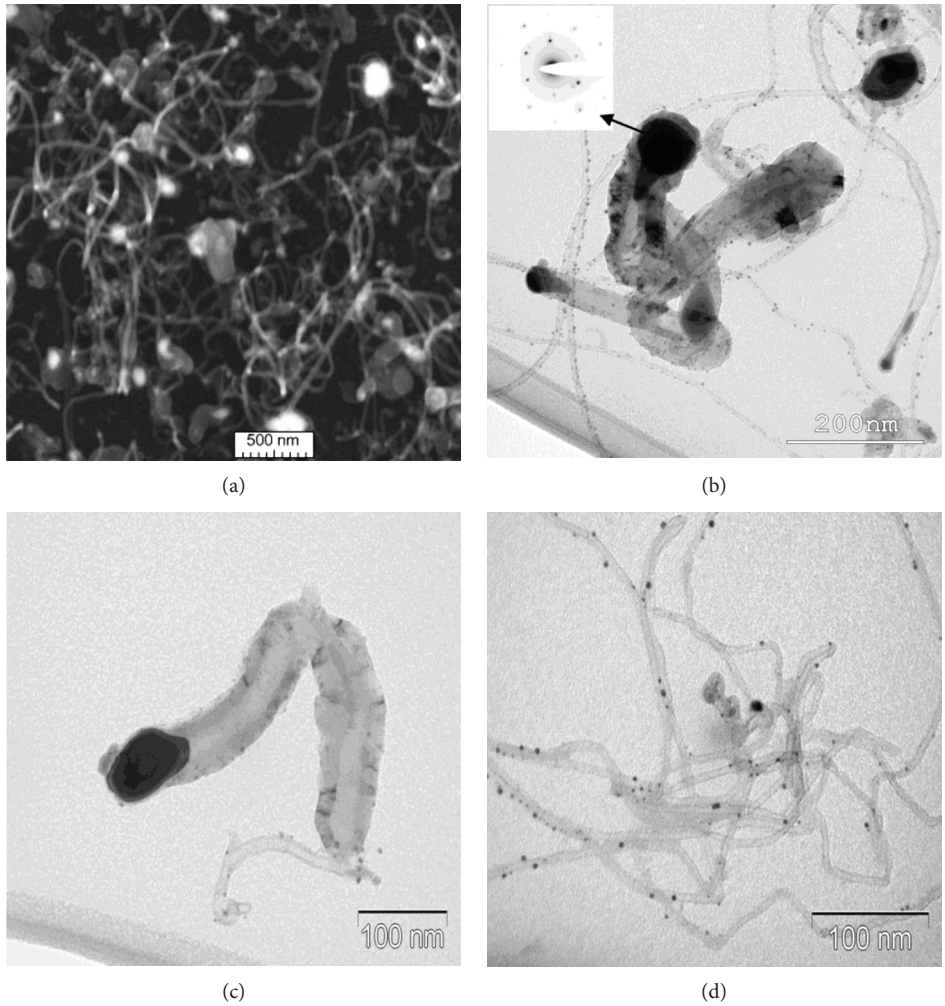

(a) (b)

(c) (d)

Figure 3: SEM (a) and TEM (b, c, d) micrographs of the CNT600-10 sample.

degree [38]. The dependencies of the $I(D)/I(G)$ on the NFC growth time are shown in Figure 4(b). The disorder degree increases with increasing growth time. It can be attributed to the loss of nanoparticle catalytic activity. Less defective samples, synthesized for only 10 min at 600, 650, and 700°C, had $I(D)/I(G) = 0.88$, 0.7, and 0.44, respectively. It reveals that higher temperature had a positive effect on the NFC graphitization degree, but the role of the temperature in the suppression of defects is lower for a longer growth time.

3.2. Ammonia Gas Response Measurements of NFC Films. The sensor resistances varied in a wide range from 0.87 kΩ to 38.60 kΩ (Table 3). The highest resistance for each deposition time was obtained at 600°C. The resistance dropped from 38.60 to 2.72 kΩ (for 10 min deposition time) when the deposition temperature increased from 600 to 700°C.

The resistance variations can be explained with the help of high resolution SEM images (Figure 5) that divided the sensors into three groups. The first group is represented by only one sample CNF600-10 which possesses the highest resistance. The sensing material is composed of short carbon nanofibers connected with each other by rarely dispersed MWCNTs. The second group consists of CNF650-10, CNF600-40, and CNF600-60 samples. The length of the CNFs and CNTs increases, and it creates additional connections and forms the network with a lower sensor resistance ($R \approx 6$–9 kΩ). The third group is represented by CNF650-60, CNF700-10, CNF700-40, and CNF700-60 samples. Increasing the amount of MWCNTs enhances the formation of the conductive network between nanotubes whereas the role of carbon nanofibers becomes negligible (sensor resistance $R < 3$ kΩ). The conductive network formed during longer deposition time and with the increase of the deposition temperature, and it has a certain similarity with the formation of percolating networks. The sample in the first group can be understood as a quasi-insulating state of the network (in terms of percolation theory); the second group of samples is situated in the transition region, and the third group represents a conductive network in which resistance is weakly influenced by the further increase in deposition time and temperature.

The changes of the sensor resistance could be partially explained also by a changed defectiveness of carbon structures. Indeed, a higher nanotube graphitization degree was proved by Raman spectroscopy, i.e., lower $I(D)/I(G)$ ratio,

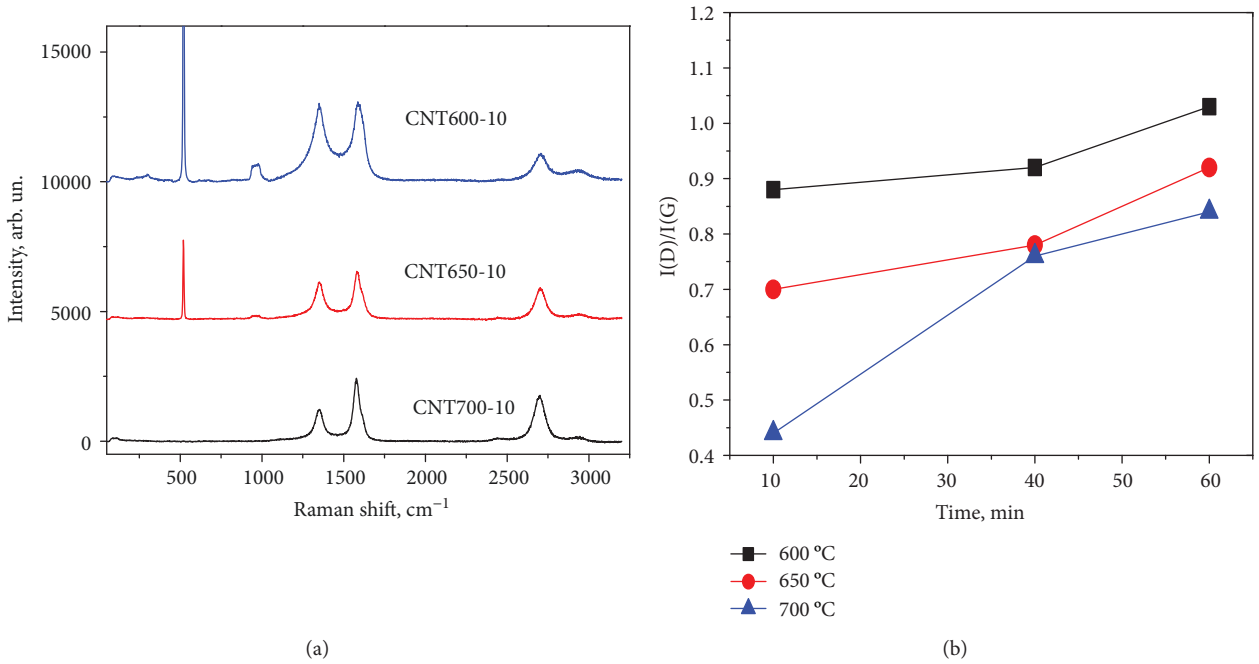

Figure 4: (a) Raman spectra of CNF600-10, CNF650-10, and CNF700-10 samples. (b) Intensity ratio $I(D)/I(G)$ vs. NFC growth time.

Table 2: Raman spectroscopy data of the samples.

Sample	D peak position, cm^{-1}	D peak FWHM, cm^{-1}	G peak position, cm^{-1}	G peak FWHM, cm^{-1}	$I(D)/I(G)$
CNF600-10	1352	102	1590	70	0.88
CNF600-40	1350	150	1593	73	0.92
CNF600-60	1350	125	1594	71	1.03
CNF650-10	1350	80	1586	55	0.70
CNF650-40	1349	84	1587	64	0.78
CNF650-60	1351	158	1592	72	0.92
CNF700-10	1349	71	1581	44	0.44
CNF700-40	1352	79	1589	62	0.76
CNF700-60	1350	82	1586	66	0.84

when the temperature during the growth was increased from 600 to 650 and 700°C (Figure 4(b)). However, the sensor resistances did not increase with increasing growth time although $I(D)/I(G)$ was higher. The increased time resulted in the deposition of higher amount of interconnecting long MWCNTs, and it had much stronger influence on the sensor resistance that dropped significantly for 40 min of the growth, especially for 600°C.

It is worth noting that according to chemical equipment and plasma equipment in industry, it is possible to carry out growing of CNTs on large wafers. Moreover, a CVD process is a very simple way for CNT growth, and it is appropriate for practical application. The processes with a floating catalyst for the deposition of iron nanoparticles are also successively used for plasma-enhanced CVD of nanoparticles for subsequent growth of CNTs. The possibility to control the growth time and deposition temperature is an advantage of the process used in this paper, because it is possible to obtain the defined resistance of the sensing layer that makes the process flexible and favorable for industry.

3.3. Ammonia Adsorption on Carbon Nanostructured Films. All the sensors exhibited increased resistance upon ammonia exposure. The increase of the NFC sensor resistance during an ammonia adsorption has been explained on the basis of the hole depletion in p-type MWCNTs [39, 40].

Adsorbed ammonia molecules donate electrons to CNTs inducing a decrease of charge carriers (holes). The same effect was observed for p-type SWCNTs [40]. The resistance of CNF600-10, 38.60 kΩ, was quite high for the MWCNT-based sensors [40, 41], but this sample exhibited the highest response, 2.8% to 500 ppm at room temperature (Figure 6). In addition, the sample CNF600-40 exhibited the response comparable to CNF600-10, e.g., 2.5% at 500 ppm (room temperature). Comparing results of Raman spectroscopy

Table 3: Summary of sensor properties. Sensor resistances at room temperature and 200°C are denoted R_{RT} and $R_{200°C}$, respectively. The sensor responses, $S_{100\ ppm}$, $S_{250\ ppm}$, and $S_{500\ ppm}$ to 100, 250, and 500 ppm of ammonia, respectively, at room temperature (RT) and 200°C were calculated as $\Delta R/R_0$.

Sample	R_{RT}, Ω	$R_{200°C}$, Ω	$S_{100\ ppm}$, %		$S_{250\ ppm}$, %		$S_{500\ ppm}$, %	
			RT	200°C	RT	200°C	RT	200°C
CNF600-10	38600	24100	1.8	1.1	2.4	1.4	2.8	2.1
CNF600-40	8940	2670	1.8	0.7	2.3	1.4	2.5	1.9
CNF600-60	8610	2580	0.6	1.1	0.8	n/a[1]	1.1	n/a[1]
CNF650-10	6860	4380	1.2	0.5	1.7	0.7	2.0	1.1
CNF650-40	2660	800	0.4	0.1	0.7	0.2	1.0	0.2
CNF650-60	1680	670	0.6	0.1	0.8	0.2	0.9	0.3
CNF700-10	2720	1340	0.4	0.4	0.6	0.7	0.7	1.1
CNF700-40	1420	530	0.3	0.2	0.4	0.4	0.5	0.5
CNF700-60	870	440	0.1	n/a[1]	0.2	n/a[1]	0.2	n/a[1]

[1]The sensor response was comparable with noise.

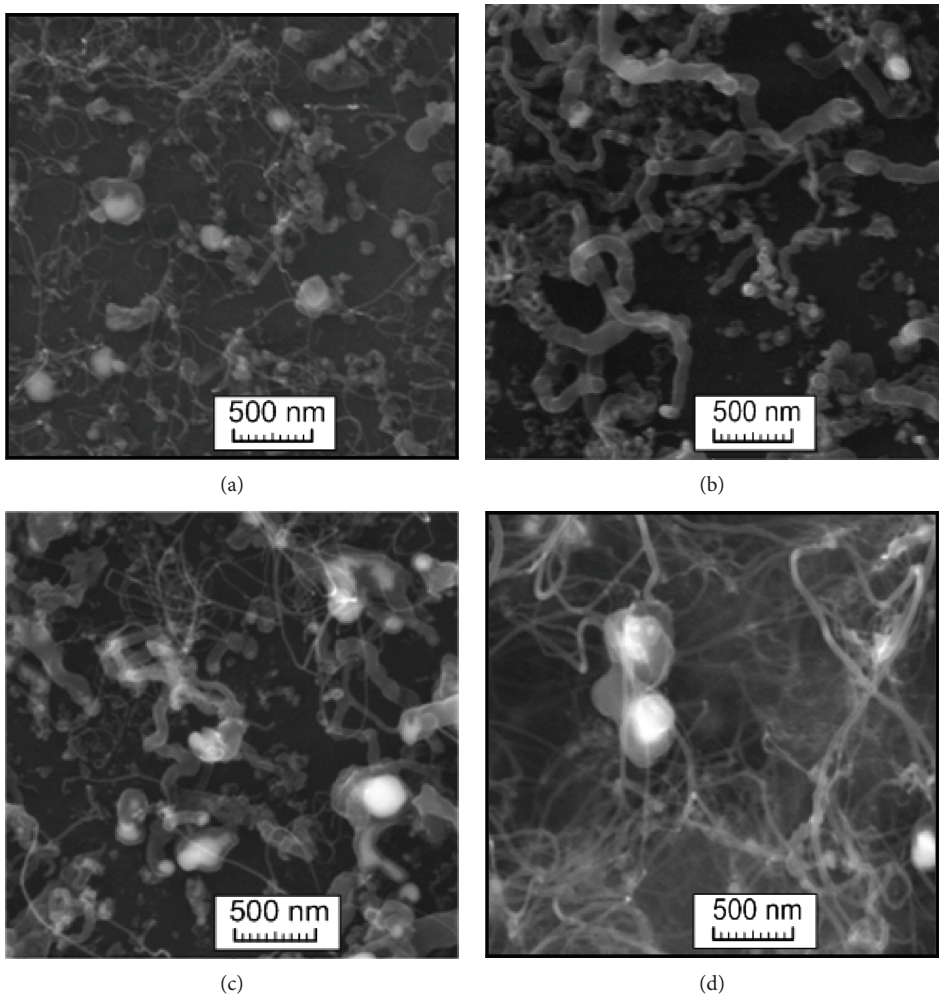

(a) (b) (c) (d)

Figure 5: SEM images of NFCs: (a) CNF600-10 (sample with the highest resistance), (b) CNF600-40 and (c) CNF650-10 (samples from the group with medium resistance), (d) CNF700-10 (sample from the group with the lowest resistance).

(Figure 4(b)), SEM images (Figure 5), and sensor resistance (Table 3), it can be concluded that the sensor response is mostly linked to the microstructure and high sensor resistance. The high resistance sensors possessed low charge carrier concentration, and thus, they were more sensitive to any change of NH_3 adsorption. Mishra et al. [32] supposed

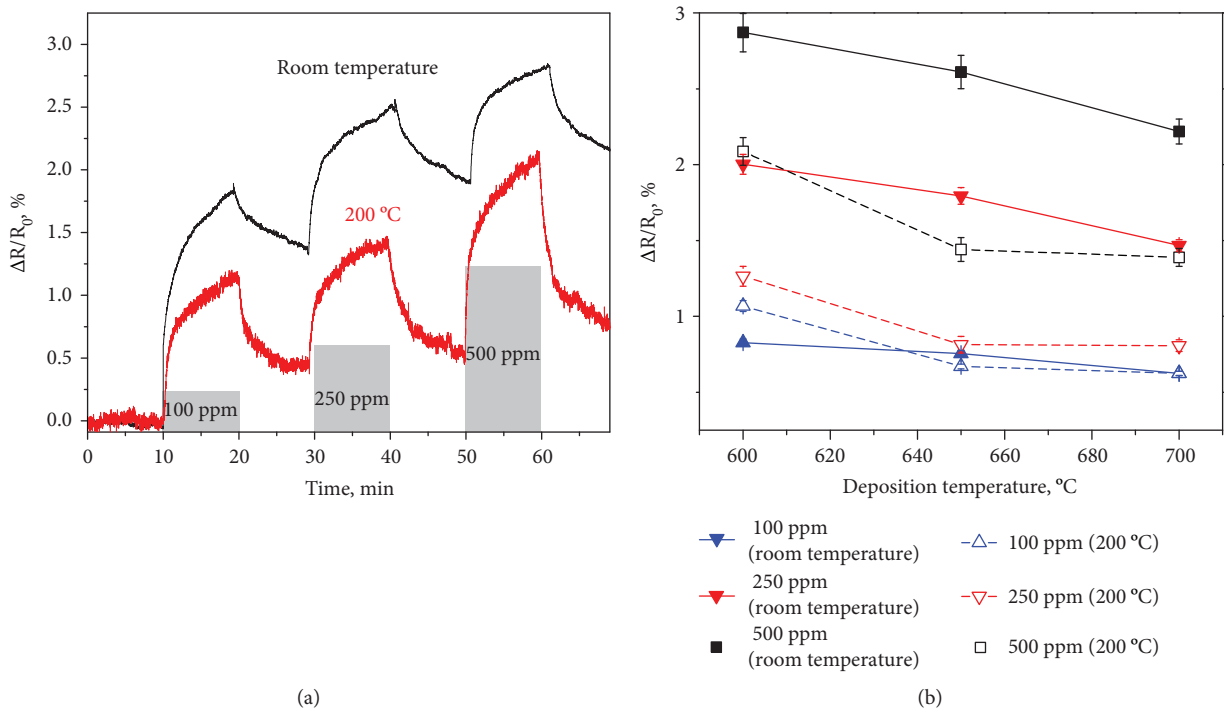

Figure 6: (a) Response curves of the CNF600-10 sample to ammonia at room temperature and 200°C. Ammonia exposure period and its concentration are depicted in the graph. (b) CNF600-10 sensor response at the room temperature (solid symbols) and 200°C (open symbols) as function of the NFC deposition temperature for the deposition time of 10 min.

that the increase of the disorder degree improved the sensor response because a higher defect density increased the number of active sites in which ammonia can be adsorbed. The $I(D)/I(G)$ of the five sensors from the third group (the resistance below 3 kΩ) was quite different, 0.44–0.92, but their response did not prove to be dependent on it.

From structural studies and ammonia adsorption characterization, one can conclude that not only properties of individual components of thin film (CNFs and CNTs) but also the amount and structural arrangement of nanostructures are important for thin film response towards ammonia.

The above discussed results suggest that the response of the sensors can be increased by the decrease of the deposition temperature below 600°C. However, the preliminary experiments carried out for the NFC active layers synthesized at 500°C and 550°C, showed that these sensors possessed extremely high resistance and were almost without response to NH_3. So much reduced temperatures had a negative effect on the reduction of catalytic NPs prior to the CNT and CNF growth. It resulted in a very low yield of NFCs, and iron oxide and Fe_3C NPs were covered by carbon. It is worth noting that no iron was detected on the surface of our samples by XPS analysis even for the deposition temperature of 600°C. In this connection, the iron nanoparticles have no direct contact with ammonia and have no influence on the response from the point of adsorption. The catalytic nanoparticles can change the conductivity of carbon nanomaterials but only for carbon nanomaterials synthesized using low deposition time, e.g., 10 min, or low temperature (600°C). Their presence in the active material increases the resistance of the active layer but only for limited samples, and we supposed that it has a little effect on the sensor response, because conductivity in such materials is mainly determined by the number of contacts formed between the nanotube and nanofiber network (this effect can be treated as percolation).

The response of the sensors at 100 ppm, 250 ppm, and 500 ppm NH_3 was in the ranges of 0.1–1.8%, 0.2–2.4%, and 0.2–2.8%, respectively. In comparison with previously published results, such as Cui et al. [29] obtained the response of 2.8% for bare MWCNTs under exposure to 1% of NH_3 (i.e., 10000 ppm). Hoa et al. [42] achieved approximately 8% response to 6% of NH_3 (60000 ppm) using CNTs on anodized alumina template; our NFC thin films exhibited the 2.8% response under much lower exposure of 0.05% (500 ppm) of NH_3. This is comparable to a more expensive SWCNT-/cellulose-based sensor [16] or chemically modified CNTs reported by Randeniya et al. [4], which showed 1–2% resistance growth of an acid-treated CNT yarn sensor under 550 ppm of ammonia. The sensors discussed in this work were not surface treated, and it is expected that some surface treatment will improve further their sensing properties. We recently reported that plasma treatment of PECVD-grown CNTs could enhance their response [43].

The adsorption on ammonia on the surface can be divided into two categories: physisorption and chemisorption. Bannov et al. [43] discussed that the response curve is a combination of both categories; the first steep part is related to physisorption of ammonia on the structure surface and later, an asymptotic part to chemisorption. In case of the recovery process, the response can quickly recover by the

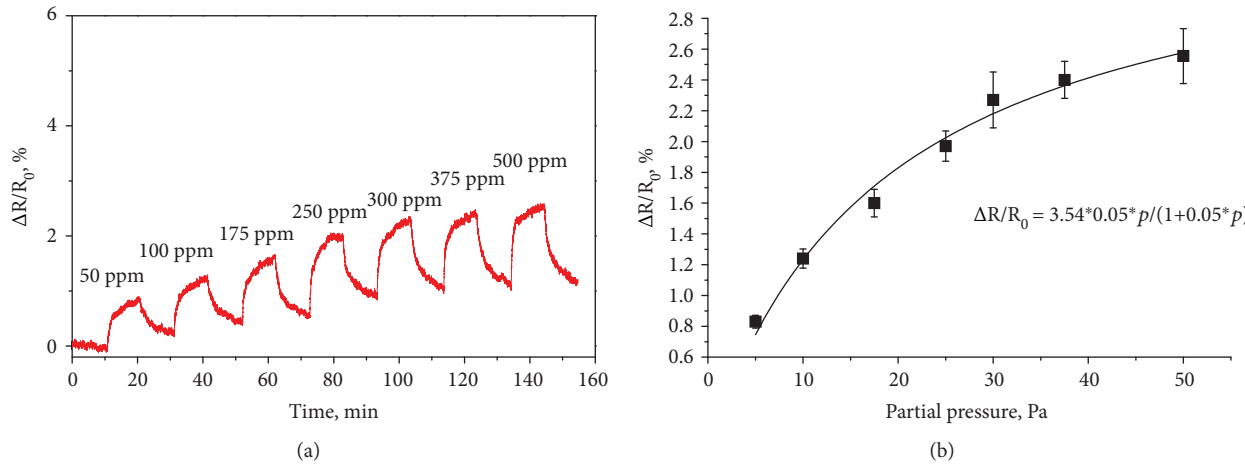

FIGURE 7: CNF600-10 response curve to NH_3 in a wide concentration range at 200°C and data fitting by Langmuir adsorption isotherm ($R^2 = 0.984$).

desorption of physisorped molecules but the recovery of chemisorbed molecules is slow or irrecoverable. For our films, we propose that the main response mechanism is physisorption and can be modelled by Langmuir isotherm. It is worth noting that it is not possible to separate chemisorption and physisorption. Nevertheless, we cannot exclude the partial chemisorption, since there is an incomplete recovery of sensor response without using heating. The use of thermal recovery makes it possible to fully carry out the desorption of ammonia molecules.

The Langmuir isotherm is usually used for the description of NH_3 adsorption on carbon materials taking into account few assumptions: each site holds each molecule, all sites are equivalent, and there is no interaction between NH_3 molecules on sites [44]. The adsorption equilibrium constant can be estimated by the following equation:

$$\theta = \theta_{\infty}\left(\frac{K \cdot p}{(1 + (K \cdot p))}\right), \quad (2)$$

where θ is the fraction of active sites covered by NH_3 (with the assumption that the value is proportional to the change of resistance), θ_{∞} is the total number of active sites, K is the adsorption equilibrium constant, and p is the partial pressure of NH_3. Results of the sample fitting by adsorption isotherm are shown in Figure 7(b). The fitting was presented taking into account that the concentration of active sites is proportional to the sensor resistance. According to the fitting, the adsorption constant of $K = 0.05\ Pa^{-1}$ was different compared with the reported one for graphene-like materials [45] ($K = 0.16\ Pa^{-1}$) and the graphene-based NH_3 sensor reported in [46].

The sensors studied can be used as industrial sensors for the determination of ammonia concentration in chemical engineering (apparatuses), oil refining, etc. The data on fitting the experimental data using Langmuir isotherm makes it possible to find the response for low NH_3 concentrations that makes it possible to predict the sensor response for 14 ppm (according to OSHA regulations) and below that is appropriate for environmental control sensors. It is worth noting that there is a necessity to control also the higher concentrations (1000–20000 ppm) for turning on the emergency ventilation in compressor rooms at the facilities used anhydrous ammonia and the sensors studied can be also used for this purpose.

3.4. Influence of the Operating Temperature on NFC Film Response and Its Recovery. NFC-based sensors possessed good response at room temperature that is an advantage as compared with semiconductor-based conventional sensors [47]. The sensors working at room temperature were also prepared using graphene-based materials. For example, Katkov et al. [45] created a fluorine-functionalized graphene sensor and reached 10.2% response to 10000 ppm of ammonia. The response 3–4% for 0.1% (1000 ppm) NH_3 in Ar was obtained on reduced graphene oxide-silver nanowires [48].

The sensor responses at room temperature and 200°C were quite different. The dependence of $\Delta R/R_0$ on the concentration had almost linear behaviour at 200°C, whereas it became nonlinear at room temperature (Figure 6(b)). The maximum response at 200°C was 2.5% in comparison with 2.8% at room temperature. The enhanced sensor response at the room temperature can be explained by the thermodynamics of adsorption. The adsorption is an exothermic process, and therefore, an increase of temperature enhances the desorption and higher temperatures (compared to room temperature) are favourable for this process. Additionally, it can be caused by weaker desorption at room temperature that lead to accumulation of small amount of ammonia on NFC surface. For example, the recovery percentage (measured after 10 min recovery in synthetic air) of the sensor CNF600-10 for 100 ppm at room temperature is only 23% in comparison with 62% at 200°C. The full adsorption-desorption cycle for wide range of concentrations of NH_3 (50–500 ppm) can be seen in Figure 7(a). We can see that although the recovery at 200°C was significantly better than at room temperature, we can observe at higher concentration saturation of the NFC thin film response an increase of background resistance.

It is worth noting that porosity of carbon nanomaterials (active material of sensor) can have an influence on the sensor response, but there is no possibility to obtain the information on the porosity of thin films because the volume of carbon nanomaterial is low enough to carry out the study of porosimetry by low-temperature nitrogen adsorption, or other techniques.

The response time of the CNF600-10 sample at room temperature was 456 s, 291 s, and 250 s for 100 ppm, 250 ppm, and 500 ppm, respectively. The increase of temperature increases the response time of the sensor to 240 s, 307 s, and 292 s, respectively. As can be seen, there is no strong dependence between concentration of ammonia and response time.

The adsorption-desorption history plays a significant role in the formation of sensor response. Therefore, the sensor response to a stepwise increase of the ammonia concentration without the recovery phase was studied for CNF600-40 in which response was very similar to CNF600-10 (Figure S3 in Supplementary Materials). The cumulative response of the CNF600-40 sample achieved at 500 ppm of ammonia was 3.5% instead of 2.5% measured after the third cycle (500 ppm) with 10 min recovery phases. The response curves showed good reproducibility, and a saturation state was not achieved during this measurement.

If the sensor recovery is required, it is necessary to employ some method, such as heating [4, 40], increasing of gas flow [40], irradiation by infrared light [49], and strong electric field [32] to accelerate it. Preliminary measurements showed that the sensor recovery performed by an air flow increase was insufficient for a complete sensor recovery. It was caused by the sensor saturation by NH_3 molecules from the previous concentration. In the previous section, the whole measurement was carried at out 200°C and it improved the sensor recovery but the response was lower in comparison to room temperature response. Since the idea of this work was to create the sensor working at room or only slightly elevated temperature, we tested temperature increase to 100°C for 3 min only during the recovery phase. The sensor recovery by this heating allowed almost a full desorption of NH_3 and achieved a good reproducibility of the sensor response (Figure 8). Recovery response of the CNF600-40 sample was stable on the level 1.1% at 100 ppm during the three cycles of ammonia exposure. In [41], the authors achieved good recovery (98.5%) only by using the heating to 150°C and increased DC bias current (3 mA) for 20 min recovery of the MWCNT-PANI sensor. The role of the bias current in our NFC sensor recovery is negligible because the bias current for the samples was $1.1 \cdot 10^{-4}$ A. The short-time sensor recovery provides more effective application of the sensor because achieving of constant response in time is very time-consuming.

As mentioned previously, we used 10 min time for adsorption and desorption in our measurement cycle. In this cycle, it was not possible to reach full response of the NFC thin film and the response was still increasing at 10 min. That is why we carried out measurement with longer exposure time of 60 min. The response curve of the steady state (CNF600-40) is shown in Figure 9. It is worth noting that

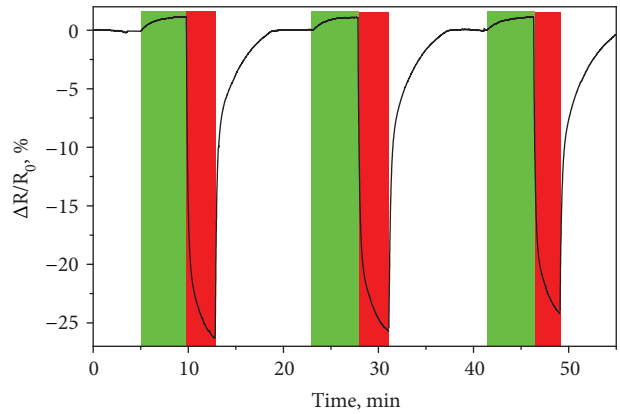

Figure 8: CNF600-40 response curve using 3 min recovery cycles (recovery temperature 100°C, recovery time 3 min), both at the room temperature (green color: exposure of NH_3; red color: thermal recovery of the sample).

even at 60 min of adsorption time, the response was still increasing for 100 and 250 ppm of NH_3 but was saturated for 500 ppm. The measurements in steady-state regime allowed achieving higher response of 3.6%, 4.1%, and 10.2% for CNF600-40 to 100 ppm, 250 ppm, and 500 ppm NH_3, respectively. The sensor response at higher durations of NH_3 exposure was several times higher than that data of 10 min exposure. Therefore, it can be concluded that longer exposure time led to higher response of the CNF thin film, but in industrial application, such time period is unpractical and short response time are required. Also in our case, much shorter exposure time, 1–2 min, was sufficient to reliably detect the presence of ammonia (Figure 9(b)).

3.5. NFC Film Response Selectivity and Influence of Humidity. An important parameter for the application of every material as a gas sensor is its selectivity, i.e., response to other gases than the selected target gas. We investigated response of our NFC thin film to H_2 and iC_4H_{10} (Figure 10(a)). These gases are frequently used in oil refining and petrochemistry. Therefore, the exhaust gases coming from apparatuses contain mainly hydrocarbons and hydrogen. The conventional process of NH_3 production by steam reforming includes them, and it is important to detect ammonia selectively.

The response to H_2 and iC_4H_{10} was almost 10 times lower than to NH_3, and the recovery was negligible. The very low recovery of the NFC film was probably caused by thermodynamics of desorption.

Another important point for real world application of gas sensors is influence of air humidity (RH). In our work, the increase of RH led to the decrease in sensor response (Figure 10(b)) and resulted in weaker desorption of NH_3. This can be explained by two processes taking place on nanostructured carbon surface in the presence of H_2O: formation of NH_4^+ ions and partial oxidation of NH_3 to NO_2 on NFC surface [50]. These processes induce the formation of holes resulting in resistance decrease.

The phenomenon of change of response for carbon nanomaterials under different relative humidities is well known,

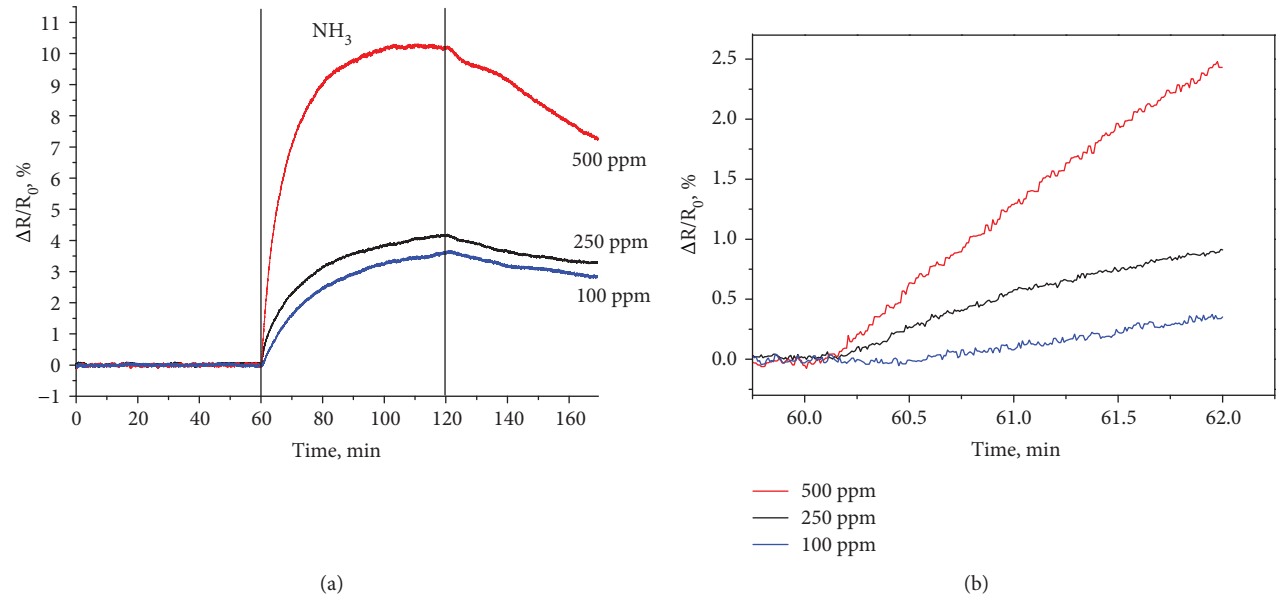

Figure 9: Steady-state sensor response curve (a) of the CNF600-40 sample (duration of NH_3 exposure was 60 min; room temperature) and extended response curve within the first minutes of contact with NH_3 for this sensor (b).

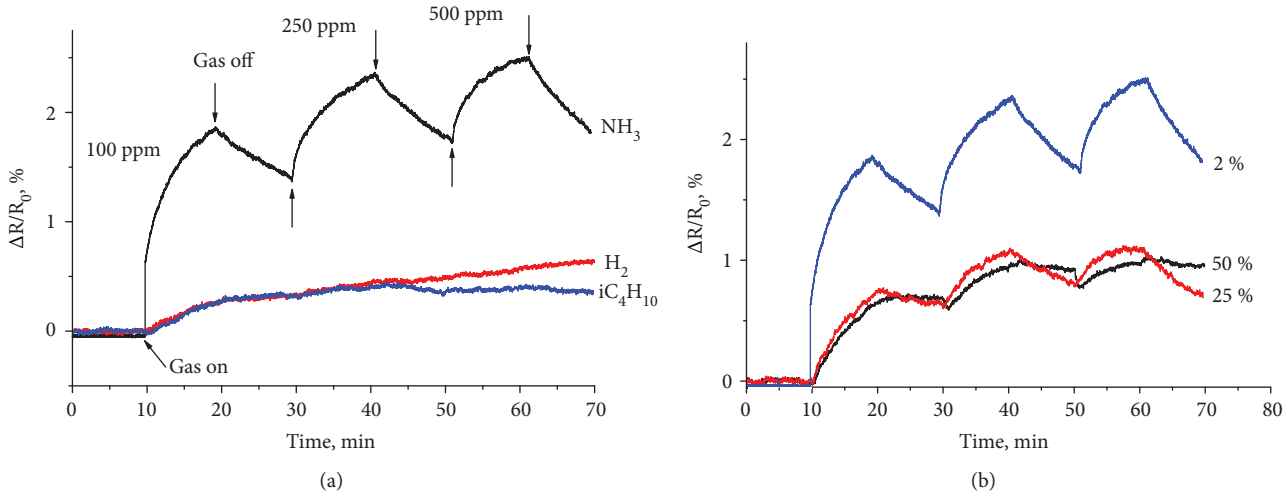

Figure 10: (a) Selectivity of the CNF600-40 sample to NH_3 in a comparison with H_2 and iC_4H_{10}. (b) Influence of RH to CNF600-40 response.

and this effect has been also found for some graphene-like materials [51]. According to chemical nature of these materials, we are not able to change the adsorption of moisture during operating the sensor but it is possible to create the calibration curves, sensor response vs. RH, and embed the relative humidity sensor for the correction of data coming from the NH_3 sensor based on nanofibrous carbon. Comparing the sensors studied with conventional TGS 826 (produced by Figaro Co.), it can be found that the detection range 30–300 ppm is almost similar to our sensors whereas it allows detecting ammonia in air at ambient temperature $20 \pm 2^{\circ}C$ and $65 \pm 5\%$RH, while the active material has a relatively higher operating temperature compared to NFCs-based sensors studied in this article. As it was shown above, the sensors studied make it possible to operate under higher temperatures and a lower RH value that is favorable for NH_3 detection at the industrial facilities.

4. Conclusions

The nanofibrous carbon films were prepared by CVD on Si/SiO_2 substrates using iron catalytic nanoparticles and used as chemiresistor ammonia sensors. The prepared films contained different amounts of short bamboo-like hollow fibres and long MWCNTs depending on the deposition temperature and time. The MWCNTs were responsible for the carbon network interconnection, and their larger amount at higher temperature and longer deposition time decreased the sensor resistance from 38.60 to 0.87 kΩ. The NFC thin film resistances increased when exposed to ammonia in all

the cases, but their response varied. A decrease of the deposition time and temperature led to the 10-fold increase in sensor response. The sensor response was highest for thin films with high resistance, and the maximum response was achieved at room temperature, 2.5 and 2.8% for 500 ppm of ammonia, for the sensors deposited at 600°C for 40 and 10 min, respectively. The response was reproducible and high in comparison to other published results on bare multiwalled carbon nanotube sensors. Thin film analysis showed that the film structure as well as properties of individual CNFs influences sensor response to ammonia adsorption. Physisorption of ammonia on carbon nanostructures was identified as the main mechanism of thin film resistance change. Difference between room temperature and high temperature (200°C) response and the time dependence of response curve during subsequent measurement cycles can be explained by a competing adsorption and desorption process of ammonia on carbon nanostructured surface. An improvement of the sensor performance was achieved by a short thermal heating at 100°C during the recovery phase.

Data Availability

The sensor characteristic data used to support the findings of this study are included within the article. Also, the selective area diffraction patterns and scanning electron microscopy data used to support the findings of this study are included within the supplementary information file.

Conflicts of Interest

The authors declare that there is no conflict of interest regarding the publication of this paper.

Acknowledgments

This research has been supported by the project LO1411 (NPU I) funded by Ministry of Education, Youth and Sports of the Czech Republic. This work was carried out under the project CEITEC 2020 (LQ1601) with financial support from the Ministry of Education, Youth and Sports of the Czech Republic under the National Sustainability Programme II. Additionally, this work was financed by the National Sustainability Program under the grant LO1401 for the research infrastructure of the SIX Center. We would like to thank Dr. Dušan Hemzal for Raman spectroscopy and Dr. Zuzana Pokorná for SEM of nanoparticles. AGB also acknowledged the Stipend of President of Russian Federation for Young Researchers (SP-547.2018.1) and the program within the framework of the strategic development of the Novosibirsk State Technical University (project code no. 1).

Supplementary Materials

Supplementary materials include selective area diffraction (SAD) patterns of catalyst used for nanofibrous carbon (NFC) synthesis which show the predominant presence of the γ-Fe_2O_3 phase among the nanoparticles (Figure S1). SEM micrographs of all the NFC samples prepared at different temperatures and deposition times are compared in Figure S2: (a) CNF600-10, (b) CNF600-40, (c) CNF600-60, (d) CNF650-10, (e) CNF650-40, (f) CNF650-60, (g) CNF700-10, (h) CNF700-40, and (i) CNF700-60. CNF600-40 response curve during stepwise increase of the NH_3 concentration in the range of 10–500 ppm (Figure S3). *(Supplementary Materials)*

References

[1] M. PEREZCABERO, "Characterization of carbon nanotubes and carbon nanofibers prepared by catalytic decomposition of acetylene in a fluidized bed reactor," *Journal of Catalysis*, vol. 215, no. 2, pp. 305–316, 2003.

[2] E. S. Snow, F. K. Perkins, E. J. Houser, S. C. Badescu, and T. L. Reinecke, "Chemical detection with a single-walled carbon nanotube capacitor," *Science*, vol. 307, no. 5717, pp. 1942–1945, 2005.

[3] P. Slobodian, P. Riha, A. Lengalova, P. Svoboda, and P. Saha, "Multi-wall carbon nanotube networks as potential resistive gas sensors for organic vapor detection," *Carbon*, vol. 49, no. 7, pp. 2499–2507, 2011.

[4] L. K. Randeniya, P. J. Martin, A. Bendavid, and J. McDonnell, "Ammonia sensing characteristics of carbon-nanotube yarns decorated with nanocrystalline gold," *Carbon*, vol. 49, no. 15, pp. 5265–5270, 2011.

[5] C. E. Cava, R. V. Salvatierra, D. C. B. Alves, A. S. Ferlauto, A. J. G. Zarbin, and L. S. Roman, "Self-assembled films of multiwall carbon nanotubes used in gas sensors to increase the sensitivity limit for oxygen detection," *Carbon*, vol. 50, no. 5, pp. 1953–1958, 2012.

[6] J. Mäklin, T. Mustonen, K. Kordás, S. Saukko, G. Tóth, and J. Vähäkangas, "Nitric oxide gas sensors with functionalized carbon nanotubes," *Physica Status Solidi*, vol. 244, no. 11, pp. 4298–4302, 2007.

[7] W. Li and D. Kim, "Polyaniline/multiwall carbon nanotube nanocomposite for detecting aromatic hydrocarbon vapors," *Journal of Materials Science*, vol. 46, no. 6, pp. 1857–1861, 2011.

[8] O. K. Varghese, P. D. Kichambre, D. Gong, K. G. Ong, E. C. Dickey, and C. A. Grimes, "Gas sensing characteristics of multi-wall carbon nanotubes," *Sensors and Actuators B: Chemical*, vol. 81, no. 1, pp. 32–41, 2001.

[9] T. Someya, J. Small, P. Kim, C. Nuckolls, and J. T. Yardley, "Alcohol vapor sensors based on single-walled carbon nanotube field effect transistors," *Nano Letters*, vol. 3, no. 7, pp. 877–881, 2003.

[10] X. Feng, S. Irle, H. Witek, K. Morokuma, R. Vidic, and E. Borguet, "Sensitivity of ammonia interaction with single-walled carbon nanotube bundles to the presence of defect sites and functionalities," *Journal of the American Chemical Society*, vol. 127, no. 30, pp. 10533–10538, 2005.

[11] R. Mangu, S. Rajaputra, P. Clore, D. Qian, R. Andrews, and V. P. Singh, "Ammonia sensing properties of multiwalled carbon nanotubes embedded in porous alumina templates," *Materials Science and Engineering: B*, vol. 174, no. 1-3, pp. 2–8, 2010.

[12] F. Rigoni, S. Tognolini, P. Borghetti et al., "Enhancing the sensitivity of chemiresistor gas sensors based on pristine carbon nanotubes to detect low-ppb ammonia concentrations in the environment," *The Analyst*, vol. 138, no. 24, pp. 7392–7399, 2013.

[13] E. Bekyarova, M. Davis, T. Burch et al., "Chemically functionalized single-walled carbon nanotubes as ammonia sensors," *The Journal of Physical Chemistry B*, vol. 108, no. 51, pp. 19717–19720, 2004.

[14] R. M. Sidek, F. A. M. Yusof, F. M. Yasin, R. Wagiran, and F. Ahmadun, "Electrical response of multi-walled carbon nanotubes to ammonia and carbon dioxide," in *2010 IEEE International Conference on Semiconductor Electronics (ICSE2010)*, pp. 263–266, Melaka, Malaysia, 2010.

[15] J. Kombarakkaran, C. F. M. Clewett, and T. Pietraß, "Ammonia adsorption on multi-walled carbon nanotubes," *Chemical Physics Letters*, vol. 441, no. 4-6, pp. 282–285, 2007.

[16] J. W. Han, B. Kim, J. Li, and M. Meyyappan, "A carbon nanotube based ammonia sensor on cellulose paper," *RSC Advances*, vol. 4, no. 2, pp. 549–553, 2014.

[17] A. Sharma, M. Tomar, and V. Gupta, "Room temperature trace level detection of NO_2 gas using SnO_2 modified carbon nanotubes based sensor," *Journal of Materials Chemistry*, vol. 22, no. 44, p. 23608, 2012.

[18] S. Peng, K. Cho, P. Qi, and H. Dai, "Ab initio study of CNT NO_2 gas sensor," *Chemical Physics Letters*, vol. 387, no. 4-6, pp. 271–276, 2004.

[19] Z. Li, J. Li, X. Wu, S. Shuang, C. Dong, and M. M. F. Choi, "Methane sensor based on nanocomposite of palladium/multi-walled carbon nanotubes grafted with 1,6-hexanediamine," *Sensors and Actuators B: Chemical*, vol. 139, no. 2, pp. 453–459, 2009.

[20] X. Li, J. Liu, and C. Zhu, "Various characteristic of Carbon nanotubes film methane Gas sensor," in *2006 1st IEEE International Conference on Nano/Micro Engineered and Molecular Systems*, pp. 1453–1456, Zhuhai, China, 2006.

[21] P. Samarasekara, "Hydrogen and methane gas sensors synthesis of multi-walled carbon nanotubes," *Chinese Journal of Physics*, vol. 47, pp. 361–369, 2009.

[22] H. Dai, P. Xiao, and Q. Lou, "Application of SnO_2/MWCNTs nanocomposite for SF_6 decomposition gas sensor," *Physica Status Solidi*, vol. 208, no. 7, pp. 1714–1717, 2011.

[23] H. Li, J. Zhang, G. Li et al., "Triton assisted fabrication of uniform semiconducting single-walled carbon nanotube networks for highly sensitive gas sensors," *Carbon*, vol. 66, pp. 369–376, 2014.

[24] J. Mäklin, T. Mustonen, N. Halonen et al., "Inkjet printed resistive and chemical-FET carbon nanotube gas sensors," *Physica Status Solidi*, vol. 245, no. 10, pp. 2335–2338, 2008.

[25] F. Mendoza, D. M. Hernández, V. Makarov, E. Febus, B. R. Weiner, and G. Morell, "Room temperature gas sensor based on tin dioxide-carbon nanotubes composite films," *Sensors and Actuators B: Chemical*, vol. 190, pp. 227–233, 2014.

[26] K. Ong and C. Grimes, "A carbon nanotube-based sensor for CO_2 monitoring," *Sensors*, vol. 1, no. 6, pp. 193–205, 2001.

[27] M. O. Ansari, S. P. Ansari, S. K. Yadav, T. Anwer, M. H. Cho, and F. Mohammad, "Ammonia vapor sensing and electrical properties of fibrous multi-walled carbon nanotube/polyaniline nanocomposites prepared in presence of cetyltrimethylammonium bromide," *Journal of Industrial and Engineering Chemistry*, vol. 20, no. 4, pp. 2010–2017, 2014.

[28] P. Teerapanich, M. T. Z. Myint, C. M. Joseph, G. L. Hornyak, and J. Dutta, "Development and improvement of carbon nanotube-based ammonia gas sensors using ink-jet printed interdigitated electrodes," *IEEE Transactions on Nanotechnology*, vol. 12, no. 2, pp. 255–262, 2013.

[29] S. Cui, H. Pu, G. Lu et al., "Fast and selective room-temperature ammonia sensors using silver nanocrystal-functionalized carbon nanotubes," *ACS Applied Materials & Interfaces*, vol. 4, no. 9, pp. 4898–4904, 2012.

[30] G. Miao, W. Kai-hua, X. Ying, W. Ren-hui, and P. Min, *For NH_3 Detection at Room Temperature*, 2010.

[31] J. Huang, J. Wang, C. Gu, K. Yu, F. Meng, and J. Liu, "A novel highly sensitive gas ionization sensor for ammonia detection," *Sensors and Actuators A: Physical*, vol. 150, no. 2, pp. 218–223, 2009.

[32] P. Mishra, P. Balyan, Harsh, and S. S. Islam, "Role of electric field on sensing mechanism of carbon nanotube based ammonia gas sensor," *Sensor Letters*, vol. 11, no. 8, pp. 1460–1464, 2013.

[33] M. Meyyappan, "Carbon nanotube-based chemical sensors," *Small*, vol. 12, no. 16, pp. 2118–2129, 2016.

[34] P. Synek, O. Jašek, and L. Zajíčková, "Study of microwave torch plasmachemical synthesis of iron oxide nanoparticles focused on the analysis of phase composition," *Plasma Chemistry and Plasma Processing*, vol. 34, no. 2, pp. 327–341, 2014.

[35] P. Synek, O. Jašek, L. Zajíčková, B. David, V. Kudrle, and N. Pizúrová, "Plasmachemical synthesis of maghemite nanoparticles in atmospheric pressure microwave torch," *Materials Letters*, vol. 65, no. 6, pp. 982–984, 2011.

[36] G. G. Kuvshinov, I. S. Chukanov, Y. L. Krutsky, V. V. Ochkov, V. I. Zaikovskii, and D. G. Kuvshinov, "Changes in the properties of fibrous nanocarbons during high temperature heat treatment," *Carbon*, vol. 47, no. 1, pp. 215–225, 2009.

[37] V. L. Kuznetsov, A. N. Usoltseva, A. L. Chuvilin, E. D. Obraztsova, and J.-M. Bonard, "Thermodynamic analysis of nucleation of carbon deposits on metal particles and its implications for the growth of carbon nanotubes," *Physical Review B*, vol. 64, no. 23, 2001.

[38] A. C. Ferrari and J. Robertson, "Interpretation of Raman spectra of disordered and amorphous carbon," *Physical Review B*, vol. 61, no. 20, pp. 14095–14107, 2000.

[39] Y. Lu, J. Li, J. Han et al., "Room temperature methane detection using palladium loaded single-walled carbon nanotube sensors," *Chemical Physics Letters*, vol. 391, no. 4-6, pp. 344–348, 2004.

[40] N. H. Quang, M. Van Trinh, B.-H. Lee, and J.-S. Huh, "Effect of NH_3 gas on the electrical properties of single-walled carbon nanotube bundles," *Sensors and Actuators B: Chemical*, vol. 113, no. 1, pp. 341–346, 2006.

[41] S. Sharma, S. Hussain, S. Singh, and S. S. Islam, "MWCNT-conducting polymer composite based ammonia gas sensors: a new approach for complete recovery process," *Sensors and Actuators B: Chemical*, vol. 194, pp. 213–219, 2014.

[42] N. D. Hoa, N. Van Quy, Y. Cho, and D. Kim, "An ammonia gas sensor based on non-catalytically synthesized carbon nanotubes on an anodic aluminum oxide template," *Sensors and Actuators B: Chemical*, vol. 127, no. 2, pp. 447–454, 2007.

[43] A. Bannov, J. Prášek, O. Jašek, and L. Zajíčková, "Investigation of pristine graphite oxide as room-temperature chemiresistive ammonia gas sensing material," *Sensors*, vol. 17, no. 2, p. 320, 2017.

[44] I. Langmuir, "The adsorption of gases on plane surfaces of glass, mica and platinum," *Journal of the American Chemical Society*, vol. 40, no. 9, pp. 1361–1403, 1918.

[45] M. V. Katkov, V. I. Sysoev, A. V. Gusel'nikov, I. P. Asanov, L. G. Bulusheva, and A. V. Okotrub, "A backside fluorine-functionalized graphene layer for ammonia detection," *Physical Chemistry Chemical Physics*, vol. 17, no. 1, pp. 444–450, 2015.

[46] F. Yavari, E. Castillo, H. Gullapalli, P. M. Ajayan, and N. Koratkar, "High sensitivity detection of NO_2 and NH_3 in air using chemical vapor deposition grown graphene," *Applied Physics Letters*, vol. 100, no. 20, article 203120, 2012.

[47] P. Heszler, Z. Gingl, R. Mingesz et al., "Drift effect of fluctuation enhanced gas sensing on carbon nanotube sensors," *Physica Status Solidi*, vol. 245, no. 10, pp. 2343–2346, 2008.

[48] Q. T. Tran, T. M. H. Huynh, D. T. Tong, V. T. Tran, and N. D. Nguyen, "Synthesis and application of graphene–silver nanowires composite for ammonia gas sensing," *Advances in Natural Sciences: Nanoscience and Nanotechnology*, vol. 4, no. 4, article 045012, 2013.

[49] M. Gautam and A. H. Jayatissa, "Ammonia gas sensing behavior of graphene surface decorated with gold nanoparticles," *Solid-State Electronics*, vol. 78, pp. 159–165, 2012.

[50] N. A. Travlou, E. Rodríguez-Castellón, and T. J. Bandosz, "Sensing of NH_3 on heterogeneous nanoporous carbons in the presence of humidity," *Carbon*, vol. 100, pp. 64–73, 2016.

[51] T. J. Bandosz, "Towards understanding reactive adsorption of small molecule toxic gases on carbonaceous materials," *Catalysis Today*, vol. 186, no. 1, pp. 20–28, 2012.